34th Annual International Conference of the IEEE EMBS
San Diego, California USA, 28 August - 1 September, 2012

Effect of saccular aneurysm and parent artery morphology on hemodynamics of cerebral bifurcation aneurysms

A. Farnoush *Member, IEEE*, Y. Qian, H. Takao, Y. Murayama, A. Avolio

Abstract— **Morphological descriptors of aneurysms have been used to assess aneurysm rupture. This study investigated the relation between the morphological parameters and the flow related parameter of energy loss (EL). Four size indices and one shape index were assessed in idealized middle cerebral artery models with various aneurysm morphologies. Four patient-specific aneurysms (2 ruptured, 2 unruptured) were virtually manipulated by removing the aneurysms from their parent arteries and merging them with the idealized bifurcation models. EL was calculated from the energy difference between inflow and outflow. The results indicate that among size indices, EL is mostly dependent on bottleneck factor and less dependent on the aspect ratio. Results also showed that there is a direct relationship between nonsphericity index (NSI) and EL in manipulated models. No specific correlation was found between EL and NSI in patient-specific models.**

I. Introduction

Risk assessment of aneurysm rupture is increasing in importance with rising prevalence of risk of rupture, currently estimated between 2% [1] and 5% [2]. Morphological analysis of aneurysms has been an area of interest for many years owing to its high feasibility with the use of CT scans and MRI measurements.

Previous studies followed two different approaches to investigate this issue. The first group focused on analyzing aneurysm morphology to discriminate between ruptured and unruptured aneurysms. These variables were classified as size and shape indices and used by Raghavan *et al* to evaluate the status of 27 patients in a blinded fashion [3]. The second group concentrated on the relation between hemodynamic parameters such as wall shear stress (WSS) and morphological parameters[4], suggesting that size ratio combined with WSS and oscillatory shear index are associated with aneurysm rupture.

In a study of 4 ruptured and 26 unruptured internal carotid artery-posterior communicating artery (ICA -PcomA) aneurysms, it has been found that the energy loss (EL) of ruptured cases was 5 times higher than that of unruptured cases [5]. In a study of 50 middle cerebral artery (MCA) aneurysms and 50 side-wall ICA-PcomA aneurysms, the higher EL was found in ruptured aneurysms compared to unruptured ones [6].

As the role of aneurysm morphology variation on hemodynamic parameters related to its growth or rupture is still unclear, the aim of this study was to investigate this relation. Our hypothesis is that any vascular changes in the Circle of Willis with aneurysms that result in energy imbalance can increase the risk of aneurysm development in the long-term [7]. Therefore, various types of aneurysm morphology located at the apex of a bifurcation were created based on existing size and shape indices in an attempt to find their effect on the hemodynamic parameter, EL. To obtain insight concerning the relationship between parent artery morphology and hemodynamics, EL was evaluated in both patient-specific and virtually manipulated models for 2 ruptured and 2 unruptured MCA aneurysms.

A.Farnoush, Y. Qian and A. Avolio are with the Australian School of Advanced Medicine, Macquarie University, Australia (email: azadeh.farnoush@students.mq.edu.au, yi.qian@mq.edu.au, alberto.avolio @mq.edu.au). H. Takao and Y. Murayama are with Jikei University School of Medicine. (email: takao@jikei.ac.jp and ymurayama@jikei.ac.jp)

II. Methodology

A. Idealized bifurcation model

The morphology of the aneurysms located at the apex of the MCA was studied by using the morphology and shape variables as described in Table I and Fig. 1a.

The neck diameter was set to 4 mm to evaluate BL, AR and H/D_{max} except for the BN model. D_{max} ranged from 6 mm to 8.4 mm to evaluate the height to D_{max} ratio where H_b varied from 2.1 mm to 6.3 mm for simulation of BL. Aneurysm of 8.4 mm in size was selected for BL and H/D_{max} models. The 180° bifurcation angle was considered for all simulations where the parent artery morphology (distal outlet diameters = 2 mm; parent artery diameter = 4 mm) [8] was kept constant throughout this study.

Table I: Morphological descriptors of MCA aneurysms.

Parameter	Description	Parameter	Description
H	Aneurysm size	Aspect ratio (**AR**)	H/N
D_{max}	Maximum diameter	Bulge location (**BL**)	H_b/H
N	Neck Width	Bottleneck factor (**BN**)	D_{max}/N
H_b	height of the maximum diameter from the neck plane	Height to maximum diameter	H/D_{max}
S	Aneurysm sac area	Nonsphericity (**NSI**)	
V	Aneurysm volume	$NSI=1-(18\pi)^{1/3}(V/S)^{2/3}$	

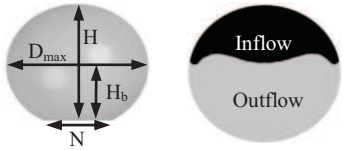

Figure 1. a) Schematic illustration of aneurysm morphology parameter,b) cross sectional area of aneurysm neck with inflow and outflow area.

Two scenarios were studied for evaluation of BN as follows:

1) BN I: aneurysm size was kept constant at 7.4 mm and the neck width ranged from 3.5 mm to 6 mm. Thus, BN and AR varied from 1.4 to 2.2 and 1.2 to 2.1, respectively.

2) BN II: aneurysm size increased from 4.3 mm to 12.6 mm as neck width altered from 3.5 mm to 6 mm, respectively. For comparison, the aneurysm size was selected so as to obtain similar AR and BN to the previous scenario.

To study the effect of AR, the aneurysm size ranged from 5.3 mm to 8.4 mm with AR of 1.3 to 2.1, respectively. However, a variety of patient–specific aneurysm morphologies indicated that the enlargement of the aneurysm does not follow a regular pattern. In the current study, it was assumed that the growth of the aneurysm is associated with the two following scenarios:

i. AR I: Increasing of AR by assuming that the spherical shape of the aneurysm did not change.

ii. AR II: Aneurysm grows with constant D_{max} width which was located at the center of the aneurysm for every ARs. Thus, the larger the aneurysm, the more likely it is to be egg-shaped.

To investigate how the deviation of the aneurysm surface from a spherical shape (NSI) affects the hemodynamic parameters, the geometries of 4 patient-specific aneurysms were virtually manipulated to eliminate the influence of other parameters including the effect of parent artery and branch diameters. Virtual manipulation was performed by removing the aneurysm sac and its neck from the parent vessel and merging it with the apex of the idealized parent vessel (Fig. 2). The ICEM CFD 13.0 software was used to generate each model.

B. Computational modeling

A finite volume code, ANSYS 13.0 was used to solve the Navier-Stokes equations by performing a second order differencing scheme for all simulation. The blood was assumed to be steady, incompressible and Newtonian fluid [9] with constant physical properties (density = 1050 kg/m^3; dynamic viscosity = 0.0035 *Pa.s*). The steady flow condition of 218 ml/min (peak flow rate in the MCA [10]) was applied at the inlet. The traction free boundary condition [11] and no-slip condition were imposed on outlets and along the artery and aneurysm wall, respectively. The arterial wall deformation was assumed to be negligible.

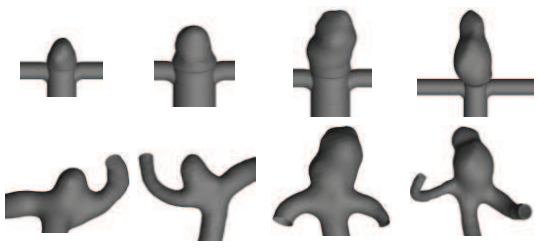

Figure 2. First row: manipulated patient-specific models; second row: patient specific models

To approach the fully-developed state [12] and avoid the effect of boundary condition location [13], inlet and outlet boundaries were located 80 mm and 100 mm from the apex of bifurcation. An unstructured tetrahedral and prismatic mesh has been utilized in the discretisation of the models, where the grid independency test recommended the average of 1.5×10^6 elements for the smallest aneurysm size. The difference between energy transport to the aneurysm by influx and energy removed from the aneurysm by outflow was defined as energy loss. A section plane perpendicular to the parent artery at the apex of the bifurcation was considered as the aneurysm neck.

The inflow and outflow area was defined as a portion of neck with positive and negative velocities, respectively (Fig.1b). Here, EL can be calculated by the following formula:

$$\text{Energy loss (EL)} = E_{\text{inlet}} - E_{\text{outlet}} \quad (1)$$

$$EL = \underbrace{\sum\left(P_i + \rho\frac{1}{2}v_i^2\right)Q_i}_{E_{inlet}} - \underbrace{\sum\left(P_o + \rho\frac{1}{2}v_o^2\right)Q_o}_{E_{outlet}} \quad (2)$$

where *P, v* are the static pressure and velocity, respectively; *i* indicates the inflow to the aneurysm through aneurysm neck ; *o* the outflow of aneurysm through aneurysm neck. E_{inlet} and E_{outlet} are the spatially averaged energy values over the cross section of the neck. To assess the effect of parent artery anatomy, both manipulated and patient-specific models were simulated under similar boundary condition.

III. Results

A. Bulge location

BL is determined by the ratio between the heights of the maximum bulge (H_b) to the aneurysm size (H). The results showed that "pear" shape (BL > 0.5) and "beehive" shape (BL < 0.5) aneurysms [14] have the highest EL (0.13 mW) and lowest EL (0.11 mW), respectively. This can be attributed to the elevation of pressure gradient in the pear shape aneurysm which increases its EL by 11% compared with the EL of beehive shape aneurysm.

B. Height to maximum diameter

The ratio between height and D_{max} represents how close the shape of the aneurysm is to a uniform morphology such as an ellipsoid or sphere. To evaluate this parameter, the size of the aneurysm was kept constant and D_{max} reduced gradually. As a result, the shape of the aneurysm was changed from spherical (H/D_{max}=1) to more egg-shaped (H/D_{max}=1.4). The results showed that the highest EL occurs in an egg-shaped aneurysm (0.14 mW) compared to a spherical aneurysm (0.11 mW) (Fig. 3). This can be attributed to the elevation of the pressure gradient in the egg-shaped aneurysm due to the non-uniformity of its morphology which increases the magnitude of EL accordingly.

C. Bottleneck factor

BN I: Aneurysm Size, constant; Neck width, variable

The aneurysm neck, as an interface between aneurysm and parent artery where the main flow and intra-aneurysmal flow interact with each other, has a major role on fluid structure inside the aneurysm. Thus, BN is defined to evaluate the ratio between aneurysm size and its neck [3]. In the first scenario, a single aneurysm was considered with different neck width. The higher difference between neck and aneurysm size, the less flow can enter the aneurysm resulting in reduction of EL by 52 % as shown in Fig. 3. Thus, the magnitude of EL was only affected by the influx of the aneurysms in this type of model.

BN II: Variables: Aneurysm Size; Neck width

In the second scenario for BN evaluation, it was assumed that the larger aneurysm has a greater neck width resulting in more flow entering the aneurysm compared with the smaller aneurysm. Thus, for similar AR and BN to the previous scenario, it has been observed that EL increased by 53 % as BN was altered from 1.4 to 2.2 (Fig.3).

D. Aspect ratio

Aspect ratio is a 2D shape index which was extensively used for discrimination of ruptured and unruptured aneurysm for the last decade. In this study, two different types of geometry (spherical and egg-shaped) were simulated in similar ARs. Fig. 3 indicated that for the first scenario (AR I), by increasing AR, the EL decreased by 4 %. This can be related to the fact that the influx and pressure gradient both reduce if the aneurysm grows spherically. An opposite pattern was seen in the egg-shaped group (AR II), where the pressure gradient increased despite the reduction of influx. Therefore, the magnitude of EL increased by 7.5 % at AR of 2.1 compared to the EL at AR of 1.3.

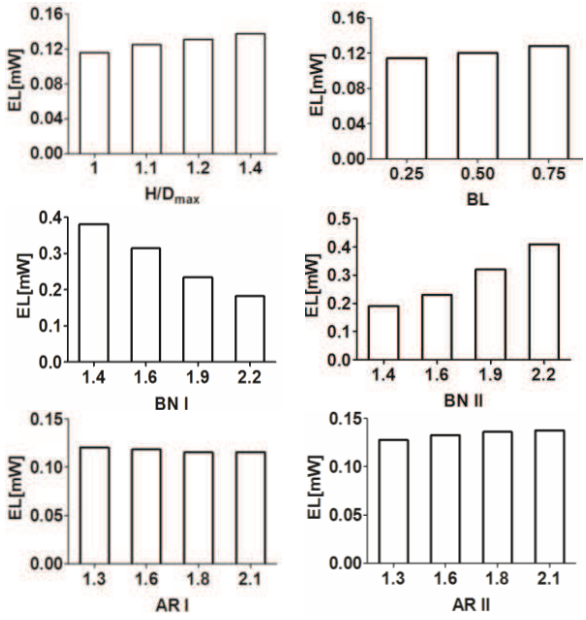

Figure 3. Calculated energy loss at various size indices of H/Dmax, BL, BN I, BN II, AR I and AR II.

E. Patient-specific model

To evaluate the patient-specific MCA aneurysms, two unruptured (case 1, 2) and two ruptured (case 3, 4) aneurysms were simulated by using similar idealized feeding parent artery and branches and patient-specific models. The size indices for all cases were measured from the CT scan of the correlated vasculature as shown in Table II.

Table II. MEASUREMENT OF SIZE INDICES AND CALCULATED ENERGY LOSS IN BOTH MANIPULATED (EL_m) AND PATIENT-SPECIFIC (EL_p) MODELS FOR 4 CASES. ALL ENERGY LOSS DIMENSIONS ARE IN mW.

	H/D_{max}	BL	BN	AR	NSI	EL_m	EL_p	Status
Case 1	0.5	0.3	1.1	0.5	0.03	0.01	0.24	U
Case 2	1.1	0.6	0.9	1.0	0.07	0.05	0.03	U
Case 3	1.4	0.3	1.2	1.7	0.165	0.07	0.38	R
Case 4	1.2	0.3	1.1	1.4	0.16	0.08	1.19	R

Results showed that EL does not follow a specific pattern regarding the H/D_{max}, BL, AR and BN values. However, if EL is plotted against NSI in manipulated model (El_m), the results indicated that as NSI increased the magnitude of EL increased by 85%. The EL of ruptured aneurysms was higher than that of unruptured ones if they were fed by similar parent arteries. Calculation of EL with patient-specific parent artery (EL_p) and same inflow showed that the highest EL still occurs in case 4 and 3, respectively, in contrast to the significant increase of EL_p in case 1 compared to the manipulated model. This can be attributed to two factors. First the flow distribution in case 1 is 66%: 34% compared to the average 85%:15% distribution for the other cases. Second, the section area of inlet in case 1 is smaller than case 2 by 28 % which increased the magnitude of velocity in case 1 by 30 %. As a result, there is a 95 % and 25 % difference between the EL calculated by two scenarios for case 1 and case 2, respectively. It should be noted that the significant increase of EL_p in case 4 is related to the smallest inlet section area compared to the other cases which increased the magnitude of velocity at inlet by 14% compared to the correlated El_m.

IV. DISCUSSION

The correlation between morphological indices of the aneurysm and hemodynamic parameter of EL was investigated in the current study. Parlea *et al* introduced 2D shape indices such as AR and BN to characterize the morphology of the aneurysm in a study of 87 single lobe cerebral aneurysms, although they could not find significant differences between the indices of ruptured and unruptured aneurysms [14]. A subsequent study of 30 patients with 67 aneurysms showed that in patients with multiple cerebral aneurysms, larger BN and height-width ratio were associated with aneurysm rupture [15]. In contrast, Raghavan *et al* suggested that due to no significant difference between BN of the ruptured and unruptured group, this parameter is more suitable in predicting the success of endovascular coiling or microsurgical clipping than aneurysm rupture assessment [3]. Our results showed that the highest change of EL occurs where the BN and neck width both increased accordingly.

However, in the case of a large aneurysm with small neck, reduction of inflow resulted in lower EL with slower blood flow velocity which increases the risk of thrombus formation [16].

Ujiie *et al* introduced AR as a clinical measurement to predict aneurysm rupture[17]. However, there is controversy regarding the role of the AR in predicting aneurysm rupture [3]. In the current study, although the EL increased in egg-shaped aneurysms in contrast to the spherical model [18], there is no strong relation between the magnitude of EL and AR if the geometry of the aneurysm conforms to 3D primitive geometric shapes. Thus, to investigate the relationship between AR, EL and aneurysm growth, the geometry of follow-up aneurysms is required even it was shown that AR is not an independent parameter to predict the risk of rupture [4].

Takao *et al* in a study of 50 side-wall ICA_PCA and 50 MCA bifurcation aneurysms [6] and Cebral *et al* in study of 210 cerebral aneurysms [19] indicated that the EL of ruptured aneurysms is higher than for unruptured ones. However, EL could not reach statistical significance. Both studies used constant mass flow rate and constant WSS at the inlet for simulation of all aneurysms, respectively. In the current study, by eliminating the effect of the parent artery and branches, our results demonstrated that the EL is significantly higher than in ruptured aneurysm compared with unruptured aneurysms with increase in NSI. In addition, modeling the aneurysms with their patient–specific parent artery gave similar results except for case 1. Thus, it can be concluded that the effect of parent artery anatomy may influence the statistical analysis of previous studies in evaluating the EL of patient-specific aneurysms with similar boundary condition.

We acknowledge that the sample size in this study is small. However, the methodology used to investigate the influence of parent artery and branch anatomy highlights the importance of this basic analysis to establish more accurate evaluation of hemodynamic parameters in patient – specific models.

V. CONCLUSION

Among the size indices of BL, AR, H/D_{max} and BN, it was found that there is a strong correlation between EL and BN with larger neck. Simulation of manipulated models for 4 patient-specific aneurysms showed that there is a direct relation between EL and NSI as both are higher in ruptured aneurysms compared to the unruptured ones. However, simulation of patient-specific models indicated that evaluating the EL based on the same boundary condition was affected by parent artery anatomy. As a result, no specific correlation was found between EL and NSI in patient-specific model. Therefore, individual estimation of the boundary condition based on the parent artery morphology is required for evaluation of EL.

ACKNOWLEDGMENT

Azadeh Farnoush is supported by Macquarie University Research Excellence Scholarship (MQRES). The project is supported by a Linkage Grant from the Australian Research Council (LP0990263), with GE Healthcare as the collaborating partner

REFERENCES

[1] G. Rinkel, M. Djibuti, A. Algra, and J. V. Gijn, "Prevalence and risk of rupture of intracranial aneurysms: a systematic review," *Stroke*, vol. 29, pp. 251-256, 1998.

[2] H. R. Winn, J. a Jane, J. Taylor, D. Kaiser, and G. W. Britz, "Prevalence of asymptomatic incidental aneurysms: review of 4568 arteriograms.," *Journal of neurosurgery*, vol. 96, no. 1, pp. 43-9, Jan. 2002.

[3] M. L. Raghavan, B. Ma, and R. E. Harbaugh, "Quantified aneurysm shape and rupture risk.," *Journal of neurosurgery*, vol. 102, no. 2, pp. 355-62, Feb. 2005.

[4] J. Xiang et al., "Hemodynamic-Morphologic Discriminants for Intracranial Aneurysm Rupture.," *Stroke; a journal of cerebral circulation*, vol. 42, no. 1, pp. 144-152, Nov. 2010.

[5] Y. Qian, H. Takao, M. Umezu, and Y. Murayama, "Risk analysis of unruptured aneurysms using computational fluid dynamics technology: preliminary results.," *AJNR. American journal of neuroradiology*, vol. 32, no. 10, pp. 1948-55, 2011.

[6] H. Takao et al., "Hemodynamic Differences Between Unruptured and Ruptured Intracranial Aneurysms During Observation.," *Stroke; a journal of cerebral circulation*, pp. 1-4, Feb. 2012.

[7] M. S. Alnaes, J. Isaksen, K.-A. Mardal, B. Romner, M. K. Morgan, and T. Ingebrigtsen, "Computation of hemodynamics in the circle of Willis.," *Stroke; a journal of cerebral circulation*, vol. 38, no. 9, pp. 2500-5, Sep. 2007.

[8] F. Umansky et al., "Microsurgical anatomy of the proximal segments of the middle cerebral artery.," *Journal of neurosurgery*, vol. 61, no. 3, pp. 458-67, Sep. 1984.

[9] Y. Hoi et al., "Effects of arterial geometry on aneurysm growth: three-dimensional computational fluid dynamics study.," *Journal of neurosurgery*, vol. 101, no. 4, pp. 676-81, Oct. 2004.

[10] M. D. Ford, N. Alperin, S. H. Lee, D. W. Holdsworth, and D. a Steinman, "Characterization of volumetric flow rate waveforms in the normal internal carotid and vertebral arteries.," *Physiological measurement*, vol. 26, no. 4, pp. 477-88, Aug. 2005.

[11] C. Karmonik, R. Klucznik, and G. Benndorf, "Comparison of velocity patterns in an AComA aneurysm measured with 2D phase contrast MRI and simulated with CFD.," *Technology and health care : official journal of the European Society for Engineering and Medicine*, vol. 16, no. 2, pp. 119-28, Jan. 2008.

[12] J. Jung, A. Hassanein, and R. W. Lyczkowski, "Hemodynamic computation using multiphase flow dynamics in a right coronary artery.," *Annals of biomedical engineering*, vol. 34, no. 3, pp. 393-407, Mar. 2006.

[13] Y. Qian, J. L. Liu, K. Itatani, K. Miyaji, and M. Umezu, "Computational Hemodynamic Analysis in Congenital Heart Disease: Simulation of the Norwood Procedure.," *Annals of biomedical engineering*, vol. 38, no. 7, pp. 2302-2313, Mar. 2010.

[14] L. Parlea, R. Fahrig, and D. Holdsworth, "An analysis of the geometry of saccular intracranial aneurysms," *American Journal of*, vol. 20, pp. 1079-1089, 1999.

[15] B. Hoh, C. Sistrom, C. Firment, and G. Fautheree, "Bottleneck factor and height-width ratio: association with ruptured aneurysms in patients with multiple cerebral aneurysms," *neurosurgery*, vol. 61, no. 4, pp. 716-723, 2007.

[16] K. Shimano, Y. Aida, and Y. Nakagawa, "Slowness of blood flow and resultant thrombus formation in cerebral aneurysms," *Journal of Biorheology*, vol. 24, no. 2, pp. 47-55, Mar. 2011.

[17] H. ; Ujiie, Y. ; Tamano, K. ; Sasaki, and T. ; Hori, "Is the Aspect Ratio a Reliable Index for Predicting the Rupture of a Saccular Aneurysm?," *Neurosurgery*, vol. 48, no. 3, pp. 495-503, 2001.

[18] A. Valencia, "Simulation of unsteady laminar flow in models of terminal aneurysm of the basilar artery," *International Journal of Computational Fluid Dynamics*, vol. 19, no. 4, pp. 337-345, May 2005.

[19] J. R. Cebral, F. Mut, J. Weir, and C. Putman, "Quantitative characterization of the hemodynamic environment in ruptured and unruptured brain aneurysms.," *AJNR. American journal of neuroradiology*, vol. 32, no. 1, pp. 145-51, Jan. 2011.